# NASA Tech Briefs

## NATIONAL AERONAUTICS AND SPACE ADMINISTRATION

- **Technology Focus**

- **Electronics/Computers**

- **Software**

- **Materials**

- **Mechanics/Machinery**

- **Manufacturing**

- **Bio-Medical**

- **Physical Sciences**

- **Information Sciences**

- **Books and Reports**

# INTRODUCTION

   Tech Briefs are short announcements of innovations originating from research and development activities of the National Aeronautics and Space Administration. They emphasize information considered likely to be transferable across industrial, regional, or disciplinary lines and are issued to encourage commercial application.

## Availability of NASA Tech Briefs and TSPs

Requests for individual Tech Briefs or for Technical Support Packages (TSPs) announced herein should be addressed to

**National Technology Transfer Center**

Telephone No. **(800) 678-6882** or via World Wide Web at **www2.nttc.edu/leads/**

Please reference the control numbers appearing at the end of each Tech Brief. Information on NASA's Innovative Partnerships Program (IPP), its documents, and services is also available at the same facility or on the World Wide Web at **http://ipp.nasa.gov**.

Innovative Partnerships Offices are located at NASA field centers to provide technology-transfer access to industrial users. Inquiries can be made by contacting NASA field centers listed below.

# NASA Field Centers and Program Offices

**Ames Research Center**
Lisa L. Lockyer
(650) 604-1754
lisa.l.lockyer@nasa.gov

**Dryden Flight Research Center**
Gregory Poteat
(661) 276-3872
greg.poteat@dfrc.nasa.gov

**Glenn Research Center**
Kathy Needham
(216) 433-2802
kathleen.k.needham@nasa.gov

**Goddard Space Flight Center**
Nona Cheeks
(301) 286-5810
nona.k.cheeks@nasa.gov

**Jet Propulsion Laboratory**
Ken Wolfenbarger
(818) 354-3821
james.k.wolfenbarger@jpl.nasa.gov

**Johnson Space Center**

Michele Brekke
(281) 483-4614
michele.a.brekke@nasa.gov

**Kennedy Space Center**
David R. Makufka
(321) 867-6227
david.r.makufka@nasa.gov

**Langley Research Center**
Martin Waszak
(757) 864-4015
martin.r.waszak@nasa.gov

**Marshall Space Flight Center**
Jim Dowdy
(256) 544-7604
jim.dowdy@msfc.nasa.gov

**Stennis Space Center**
John Bailey
(228) 688-1660
john.w.bailey@nasa.gov

**Carl Ray, Program Executive**
Small Business Innovation
Research (SBIR) & Small
Business Technology
Transfer (STTR) Programs
(202) 358-4652
carl.g.ray@nasa.gov

**Doug Comstock, Director**
Innovative Partnerships
Program Office
(202) 358-2560
doug.comstock@nasa.gov

# TECH BRIEFS

## NATIONAL AERONAUTICS AND SPACE ADMINISTRATION

# Gas Sensors Based on Coated and Doped Carbon Nanotubes

**Large specific surface areas of nanotubes could enable attainment of high sensitivities.**

*Ames Research Center, Moffett Field, California*

Efforts are underway to develop inexpensive, low-power electronic sensors, based on single-walled carbon nanotubes (SWCNTs), for measuring part-per-million and part-per-billion of selected gases (small molecules) at room temperature. Chemically unmodified SWCNTs are mostly unresponsive to typical gases that one might wish to detect. However, the electrical resistances of SWCNTs can be made to vary with concentrations of gases of interest by coating or doping the SWCNTs with suitable materials. Accordingly, the basic idea of the present development efforts is to incorporate thus-treated SWCNTs into electronic devices that measure their electrical resistances.

A typical sensor device based on this concept includes a set of interdigitated metal microelectrodes fabricated by photolithography on an electrically insulating substrate. In preparation for fabricating the SWCNT portion of such a sensor, a batch of treated (coated or doped) SWCNTs is dispersed in a solvent. The resulting suspension of SWCNTs is drop-deposited or injected onto the area containing the interdigitated electrodes. As the solvent evaporates, the SWCNTs form an irregular mesh that connects the electrodes. The density of the SWCNTs in the mesh can be varied by varying the concentration of SWCNTs in the suspension and/or the amount of suspension dropped on the electrode area. To enable acquisition of measurements for comparison and to aid in calibration, undoped SWCNTs can be similarly formed on another, identical set of interdigitated electrodes.

Examples of coating materials that have been tested thus far include chlorosulfonated polyethylene (which imparts sensitivity to chlorine) and hydroxypropyl cellulose (which imparts sensitivity to hydrogen chloride). Examples of dopants that have been tested are Pd nanoparticle doped SWCNTs (which imparts sensitivity to methane) and other dopants include clusters of nanoparticles of catalytic metals — for example, Pt
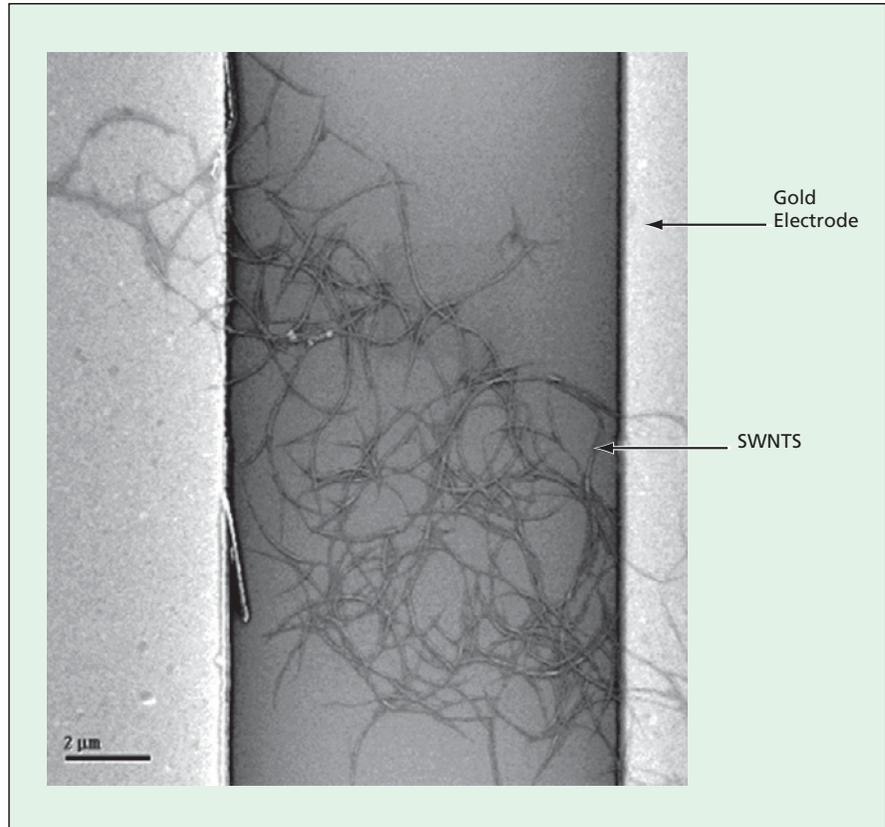


A **Mesh of SWCNTs** bridges the gap between two gold electrodes in an experimental sensor device.

and Au for sensing hydrogen and hydrocarbons or Cu and Rh for sensing nitric compounds.

Although the response of a sensor of this type is a generally monotonic function of the concentration of a gas species of interest, it is not always a linear function, sometimes it is a linear function to the logarithmic concentration. Moreover, a given sensor can be sensitive to more than one gas, and the sensitivities to different gases can be expected to differ. In a typical contemplated application, a device would incorporate multiple sensors, each tailored to maximize its response to a specific gas or family of gases, and the sensor would be operated in an environment containing a mixture of gases. The readings of the sensors would be digitized and processed by algorithms for differentiating the gases

and estimating their concentrations or at least limits on the concentration of a gas species of interest in the face of the nonlinear responses to the various gases that may be present.

This sensor technology has been developed to readily scale up for mass production with high yield and good reproducibility. The sensing device can be used for *in-situ* air monitoring, wireless network sensing, and in-line chemical detection.

*This work was done by Jing Li and Meyya Meyyappan of Ames Research Center and Yijiang Lu of Eloret Corporation.*

*This invention is owned by NASA, and a patent application has been filed. Inquiries concerning rights for the commercial use of this invention should be addressed to the Ames Technology Partnerships Division at (650) 604-2954. Refer to ARC-15566-1.*

# Tactile Robotic Topographical Mapping Without Force or Contact Sensors

## A "tap test" yields data on a succession of surface points.

*NASA's Jet Propulsion Laboratory, Pasadena, California*

A method of topographical mapping of a local solid surface within the range of motion of a robot arm is based on detection of contact between the surface and the end effector (the fixture or tool at the tip of the robot arm). The method was conceived to enable mapping of local terrain by an exploratory robot on a remote planet, without need to incorporate delicate contact switches, force sensors, a vision system, or other additional, costly hardware. The method could also be used on Earth for determining the size and shape of an unknown surface in the vicinity of a robot, perhaps in an unanticipated situation in which other means of mapping (e.g., stereoscopic imaging or laser scanning with triangulation) are not available.

The method uses control software modified to utilize the inherent capability of the robotic control system to measure the joint positions, the rates of change of the joint positions, and the electrical current demanded by the robotic arm joint actuators. The system utilizes these coordinate data and the known robot-arm kinematics to compute the position and velocity of the end effector, move the end effector along a specified trajectory, place the end effector at a specified location, and measure the electrical currents in the joint actuators. Since the joint actuator current is approximately proportional to the actuator forces and torques, a sudden rise in joint current, combined with a slowing of the joint, is a possible indication of actuator stall and surface contact. Hence, even though the robotic arm is not equipped with contact sensors, it is possible to sense contact (albeit with reduced sensitivity) as the end effector becomes stalled against a surface that one seeks to measure.

The control software algorithm is specified to move the end effector along a succession of different trajectories ending at different positions (to perform a "tap test") to measure locations of stalls of the end effector against the surface of interest, thereby acquiring the coarse topographical data on the surface. In the original application, the topographical data were used to determine safe areas for robotic excavation and sampling of soil.

*This work was done by Kevin Burke, Joseph Melko, Joel Krajewski, and Ian Cady of Caltech for NASA's Jet Propulsion Laboratory.*

*The software used in this innovation is available for commercial licensing. Please contact Karina Edmonds of the California Institute of Technology at (626) 395-2322. Refer to NPO-43922.*

# Thin-Film Magnetic-Field-Response Fluid-Level Sensor for Non-Viscous Fluids

## This sensor would be inexpensive and easy to fabricate.

*Langley Research Center, Hampton, Virginia*

An innovative method has been developed for acquiring fluid-level measurements. This method eliminates the need for the fluid-level sensor to have a physical connection to a power source or to data acquisition equipment. The complete system consists of a lightweight, thin-film magnetic-field-response fluid-level sensor (see Figure 1) and a magnetic field response recorder that was described in "Magnetic-Field-Response Measurement-Acquisition System" (LAR-16908-1), *NASA Tech Briefs*, Vol. 30, No. 6 (June 2006), page 28.

The sensor circuit is a capacitor connected to an inductor. The response recorder powers the sensor using a series of oscillating magnetic fields. Once electrically active, the sensor responds with its own harmonic magnetic field. The sensor will oscillate at its resonant electrical frequency, which is dependent upon the capacitance and inductance values of the circuit.
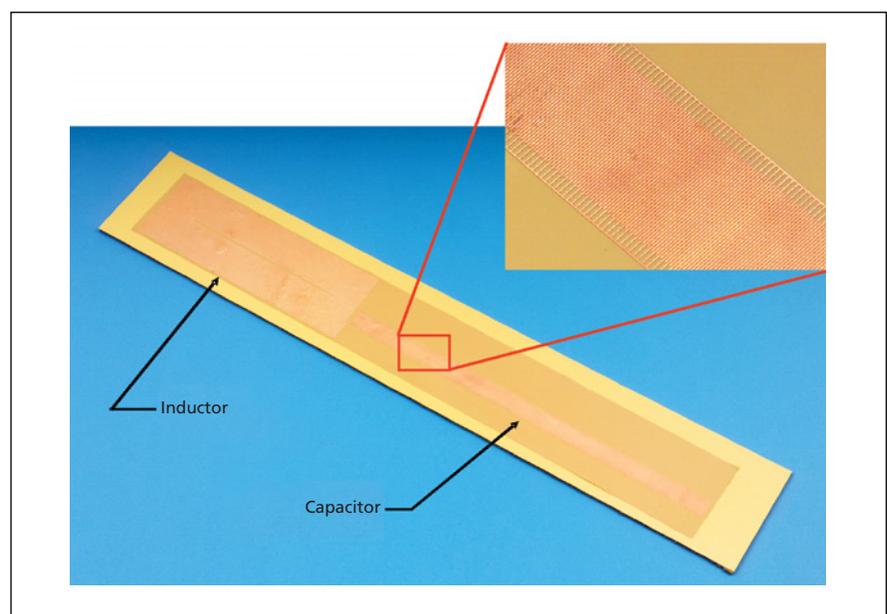


Figure 1: Thin-film magnetic field response **Fluid-Level Sensor** is a capacitor connected to an inductor to form a resonant circuit.
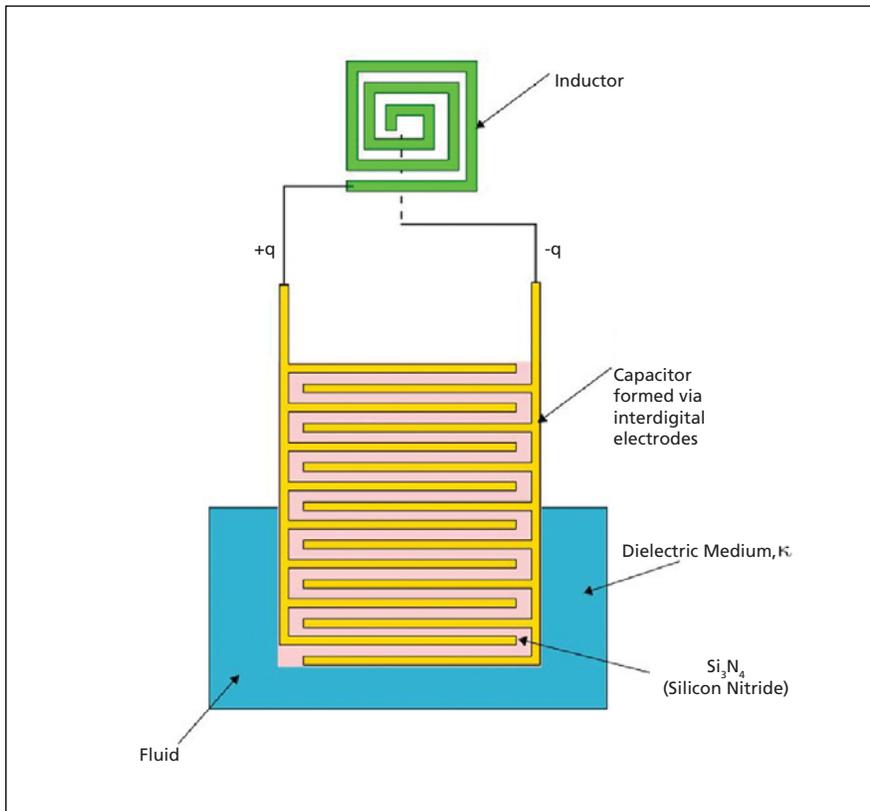
Figure 2: **Part of Capacitance** (fluid sensor) is immersed in fluid.

pacitance of $C_{free}$ when not immersed in the fluid and $C_{immersed} = \kappa C_{free}$. The advantage of this method is that it serves as a lightweight, thin-film method of measuring fluids that are non-viscous. Another advantage is that the level measurements are discretized. The sensor capacitance, $C(m)$, for a sensor having $n$ electrode pairs increases as the number of electrode pairs, $m$, in contact with the dielectric increases.

$$C(m) = (n-m)C_{free} + mC_{immersed}$$
$$= (n-m+\kappa m)C_{free}$$
$$= [n+m(\kappa-1)]C_{free}$$

When the electrodes are electrically connected to an inductor, a resonant circuit is formed having the resonant frequency of

$$\omega = \frac{1}{2\pi\sqrt{[n+m(\kappa-1)]LC_{free}}}$$

The sensor response frequency ranges from its maximum value when the capacitor is not immersed ($m=0$)

$$\omega_{max} = \frac{1}{2\pi\sqrt{nLC_{free}}}$$

to its minimum when the capacitor is completely immersed ($m=n$).

$$\omega_{min} = \frac{1}{2\pi\sqrt{m\kappa LC_{free}}}$$

*This work was done by Stanley E. Woodard, Qamar A. Shams, and Robert L. Fox of Langley Research Center and Mr. Bryant D. Taylor of SWALES Aerospace. For more information, contact the Langley Innovative Partnerships Office at (757) 864-8881. Refer to LAR-16614-1.*

The capacitance value of the sensor increases as the amount of fluid that the sensor is exposed to increases. When the energy is in the inductor, the harmonic magnetic field produced can be interrogated. The response recorder interrogates the sensor response and correlates the response frequency to fluid level.

A thin layer of silicon nitride film is deposited on interdigital electrodes as shown in Figure 2 to electrically insulate the sensor's capacitor. Silicon nitride also can be placed on the inductor. The fluid-level sensor uses interdigital electrodes for the capacitor that are electrically connected in parallel to a spiral trace inductor. The advantage of this design is that the entire sensor can be embodied as a thin film, and can be directly deposited to the inner wall of a nonconductive container for measuring non-viscous fluids.

In Figure 2, a fluid having dielectric constant, $\kappa$, is in contact with $m$ pairs of electrodes (e.g., placed in a fluid such that $m$ electrode pairs are submersed). Each electrode pair has a ca-

# Progress in Development of Improved Ion-Channel Biosensors
**Improvements in design and fabrication have been made since a previous report.**

*NASA's Jet Propulsion Laboratory, Pasadena, California*

Further improvements have recently been made in the development of the devices described in "Improved Ion-Channel Biosensors" (NPO-30710), *NASA Tech Briefs*, Vol. 28, No. 10 (October 2004), page 30. As discussed in more detail in that article, these sensors offer advantages of greater stability, greater lifetime, and individual electrical addressability, relative to prior ion-channel biosensors.

In order to give meaning to a brief description of the recent improvements, it is necessary to recapitulate a substantial portion of the text of the cited previous article. The figure depicts one sensor that incorporates the recent improvements, and can be helpful in understanding the recapitulated text, which follows:

These sensors are microfabricated from silicon and other materials compat-

ible with silicon. Typically, the sensors are fabricated in arrays in silicon wafers on glass plates. Each sensor in the array can be individually electrically addressed, without interference with its neighbors. Each sensor includes a well covered by a thin layer of silicon nitride, in which is made a pinhole for the formation of a lipid bilayer membrane. In one stage of fabrication, the lower half of the well is
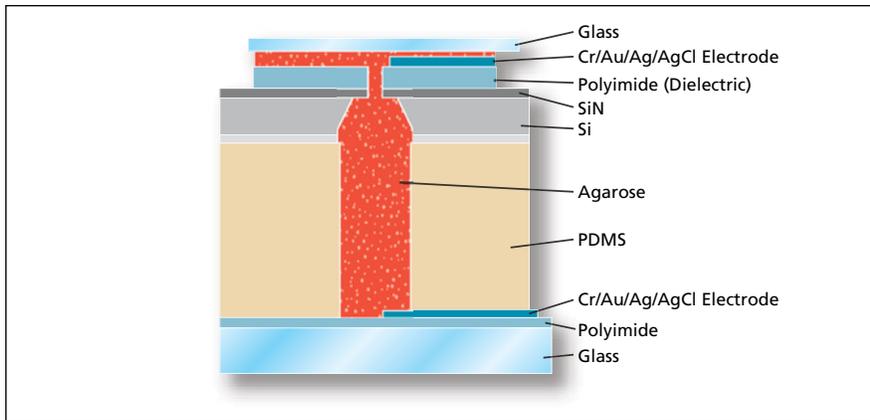
This **Simplified Cross Section**, which is not to scale, shows selected features of a sensor that incorporates recent improvements.

filled with agarose, which is allowed to harden. Then the upper half of the well is filled with a liquid electrolyte (which thereafter remains liquid) and a lipid bilayer is painted over the pinhole. The liquid contains a protein that forms an ion channel on top of the hardened agarose. The combination of enclosure in the well and support by the hardened agarose provides the stability needed to keep the membrane functional for times as long as days or even weeks.

An electrode above the well, another electrode below the well, and all the materials between the electrodes together constitute a capacitor. What is measured is the capacitive transient current in response to an applied voltage pulse. One notable feature of this sensor, in compar-ison with prior such sensors, is a relatively thick dielectric layer between the top of the well and the top electrode. This layer greatly reduces the capacitance of an aperture across which the ion channels are formed, thereby increasing the signal-to-noise ratio. The use of a relatively large aperture with agarose support makes it possible to form many ion channels instead of only one, thereby further increasing the signal-to-noise ratio and effectively increasing the size of the available ionic reservoir. The relatively large reservoir makes it possible to measure AC rather than DC. This concludes the recapitulation from the cited previous article.

The improvements include the following:

- The microfluidic channels through which agarose is wicked into the lower halves of the wells are fabricated in a reusable layer of polydimethylsiloxane [PDMS (commonly known as silicone rubber)]. This layer of PDMS forms a hermetic seal with the underlying glass plate and the overlying silicon chip, but can be removed and washed, making the array reusable.

- Before forming the lipid bilayer over the pinholes in the silicon nitride layer, the silicon nitride is coated with a self-assembled monolayer, which serves to stabilize the lipid bilayer, thereby making the array into an even more stable device.

- The lipid bilayer is formed rapidly by means of a spin-coating procedure that can be performed by a worker without special skill.

# Simulating Operation of a Complex Sensor Network

*NASA's Jet Propulsion Laboratory, Pasadena, California*

Simulation Tool for ASCTA Microsensor Network Architecture (STAMiNA) ["ASCTA" denotes the Advanced Sensors Collaborative Technology Alliance.] is a computer program for evaluating conceptual sensor networks deployed over terrain to provide military situational awareness. This or a similar program is needed because of the complexity of interactions among such diverse phenomena as sensing and communication portions of a network, deployment of sensor nodes, effects of terrain, data-fusion algorithms, and threat characteristics.

STAMiNA is built upon a commercial network-simulator engine, with extensions to include both sensing and communication models in a discrete-event simulation environment. Users can define (1) a mission environment, including terrain features; (2) objects to be sensed; (3) placements and modalities of sensors, abilities of sensors to sense objects of various types, and sensor false-alarm rates; (4) trajectories of threatening objects; (5) means of dissemination and fusion of data; and (6) various network configurations. By use of STAMiNA, one can simulate detection of tar-gets through sensing, dissemination of information by various wireless communication subsystems under various scenarios, and fusion of information, incorporating such metrics as target-detection probabilities, false-alarm rates, and communication loads, and capturing effects of terrain and threat.

# Using Transponders on the Moon to Increase Accuracy of GPS

**Ranging to the Moon would be unaffected by the terrestrial atmosphere.**

*NASA's Jet Propulsion Laboratory, Pasadena, California*

It has been proposed to place laser or radio transponders at suitably chosen locations on the Moon to increase the accuracy achievable using the Global Positioning System (GPS) or other satellite-based positioning system. The accuracy of GPS position measurements depends on the accuracy of determination of the ephemerides of the GPS satellites. These ephemerides are determined by means of ranging to and from Earth-based stations and consistency checks among the satellites. Unfortunately, ranging to and from Earth is subject to errors caused by atmospheric effects, notably including unpredictable variations in refraction.

The proposal is based on exploitation of the fact that ranging between a GPS satellite and another object outside the atmosphere is not subject to error-inducing atmospheric effects. The Moon is such an object and is a convenient place for a ranging station. The ephemeris of the Moon is well known and, unlike a GPS satellite, the Moon is massive enough that its orbit is not measurably affected by the solar wind and solar radiation.

According to the proposal, each GPS satellite would repeatedly send a short laser or radio pulse toward the Moon and the transponder(s) would respond by sending back a pulse and delay information. The GPS satellite could then compute its distance from the known position(s) of the transponder(s) on the Moon.

Because the same hemisphere of the Moon faces the Earth continuously, any transponders placed there would remain continuously or nearly continuously accessible to GPS satellites, and so only a relatively small number of transponders would be needed to provide continuous coverage. Assuming that the transponders would depend on solar power, it would be desirable to use at least two transponders, placed at diametrically opposite points on the edges of the Moon disk as seen from Earth, so that all or most of the time, at least one of them would be in sunlight.

*This work was done by Konstantin Penanen and Talso Chui of Caltech for NASA's Jet Propulsion Laboratory. For further information, contact iaoffice@jpl.nasa.gov.*
*NPO-43160*

# Controller for Driving a Piezoelectric Actuator at Resonance

**Unpredictable variations in resonance frequency are tracked.**

*NASA's Jet Propulsion Laboratory, Pasadena, California*

A digital control system based partly on an extremum-seeking control algorithm tracks the changing resonance frequency of a piezoelectric actuator or an electrically similar electromechanical device that is driven by a sinusoidal excitation signal and is required to be maintained at or near resonance in the presence of uncertain, changing external loads and disturbances. Somewhat more specifically, on the basis of measurements of the performance of the actuator, this system repeatedly estimates the resonance frequency and alters the excitation frequency as needed to keep it at or near the resonance frequency. In the original application for which this controller was developed, the piezoelectric actuator is part of an ultrasonic/sonic drill/corer. Going beyond this application, the underlying principles of design and operation are generally applicable to tracking changing resonance frequencies of heavily perturbed harmonic oscillators.

Resonance-frequency-tracking analog electronic circuits are commercially available, but are not adequate for the present purpose for several reasons:
• The input/output characteristics of analog circuits tend to drift, often necessitating recalibration, especially whenever the same controller is used in driving a different resonator.
• In the case of an actuator in a system that has multiple modes characterized by different resonance frequencies, an analog controller can tune erroneously to one of the higher-frequency modes.
• The lack of programmability of analog controllers is problematic when faults occur, and is especially problematic for preventing tuning to a higher-frequency mode.

In contrast, a digital controller can be programmed to restrict itself to a specified frequency range and to maintain stability even when the affected resonator is driven at high power and subjected to uncertain disturbances and variable loads.

The present digital control system (see figure) is implemented by means of an algorithm that comprises three main subalgorithms: a hill-climbing control algorithm, an estimation-based extremum-seeking control (ESC) algorithm, and a supervisory algorithm. The hill-climbing algorithm is useful for coarse tracking to find and remain within the vicinity of the resonance. The ESC algorithm is not capable of coarse resonance tracking, but is capable of fine resonance tracking once the estimates of parameters generated by the hill-climbing algorithm have converged sufficiently. On the basis of the parameter-estimation errors, the supervisory algorithm switches operation to whichever of the other two algorithms performs best at a given time.
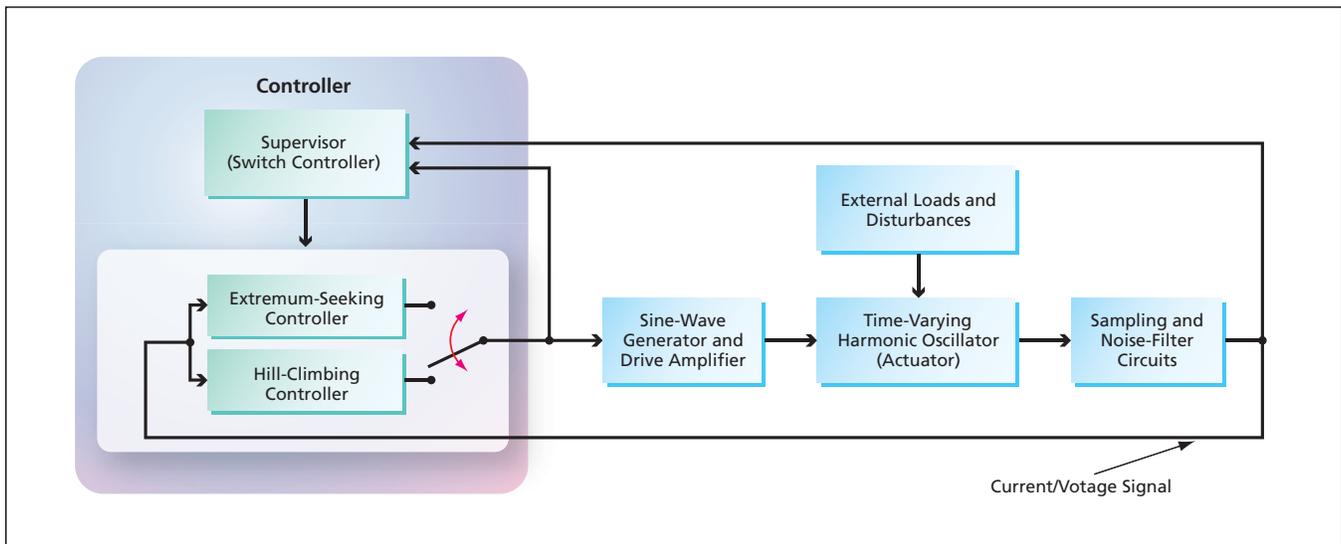
This **Resonance-Tracking Controller** includes three main subsystems that function together to effect a combination of coarse and fine frequency tracking optimized to maintain operation at a desired resonance and avoid undesired resonances.

For the purpose of the control algorithm, the performance of the actuator is quantified in terms of the ratio between the time-averaged drive-voltage amplitude and the time-averaged drive current amplitude during a sampling time period. In the hill-climbing algorithm, the excitation frequency during the next sampling period is incremented or decremented by an arbitrary fixed step. If the increment or decrement results in an increase in the current/voltage ratio, then the direction of change (increase or decrease, respectively) of frequency is accepted and another such change (increment or decrement, respectively) is made during the following sampling period. If, on the other hand, the increment or decrement results in a decrease in the current/voltage ratio, then the direction of change of frequency during the following sampling period is reversed. The

process as described thus far is repeated, causing the current/voltage performance to climb to one of the resonance peaks and eventually to oscillate about the peak. In order to prevent climbing of one of the undesired higher-frequency resonance peaks, it is necessary to choose the starting excitation frequency near the desired peak and to impose a limit on the excursion from the starting frequency.

Once the excitation frequency has begun to oscillate about the peak, the supervisory algorithm switches operation to the ESC algorithm, which uses past as well as present input/output data to make a least-squares estimate of the resonance frequency. The estimation task involves updating two scalar parameters of a quadratic model that represents the input/output map of the actuator resonance. After each sampling period, the new input/output data pair is added to

the collection of past data pairs, such that information regarding the input/output relationship of the actuator increases over time; in other words, as the input/output information comes in, the algorithm tries to improve the fit between the quadratic model near resonance and all the past input/output data up to the current time. Once the estimated parameters have converged sufficiently, the excitation frequency is updated according to a simple formula that represents a maximizer associated with the quadratic model. In the event that the estimates begin to diverge beyond a specified limit, the supervisory algorithm switches operation back to the hill-climbing algorithm.

# ◉ Coaxial Electric Heaters

## These devices can be used safely where magnetic fields are not tolerated.

*NASA's Jet Propulsion Laboratory, Pasadena, California*

Coaxial electric heaters have been conceived for use in highly sensitive instruments in which there are requirements for compact heaters but stray magnetic fields associated with heater electric currents would adversely affect operation. Such instruments include atomic clocks and magnetometers that utilize heated atomic-sample cells, wherein stray magnetic fields at picotesla

levels could introduce systematic errors into instrument readings.

A coaxial electric heater (see Figure 1) is essentially an axisymmetric coaxial cable, the outer conductor of which is deliberately made highly electrically resistive so that it can serve as a heating element. As in the cases of other axisymmetric coaxial cables, the equal-magnitude electric currents flowing in

opposite directions along the inner and outer conductors give rise to zero net magnetic field outside the outer conductor. Hence, a coaxial electric heater can be placed near an atomic-sample cell or other sensitive device.

A coaxial electric heater can be fabricated from an insulated copper wire, the copper core of which serves as the inner conductor. For example, in one ap-
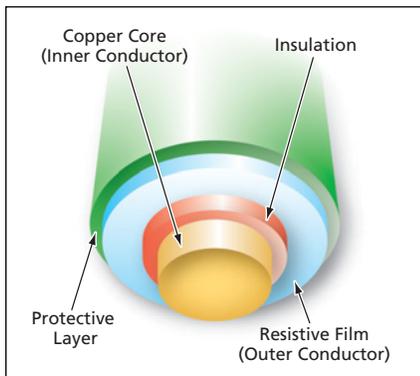
Figure 1. A **Typical Coaxial Electric Heater** as shown in cross section resembles conventional signal-transmission coaxial cables, except that its outer conductor is deliberately made highly resistive.



Figure 2. This **Coaxial Electric Heater**, shown here in a side view, was bent into a circular arc for edge heating of a circular window. This heater was made from copper wire of 0.01-in. (0.254-mm) diameter. Its resistance is about 2 kΩ.

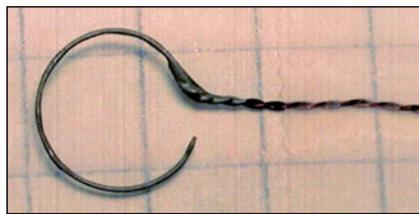proach, the insulated wire is dipped in a colloidal graphite emulsion, then the emulsion-coated wire is dried to form a thin, uniform, highly electrically resistive film that serves as the outer conductor. Then the film is coated with a protective layer of high-temperature epoxy except at the end to be electrically connected to the power supply. Next, the insulation is stripped from the wire at that end. Finally, electrical leads from the heater power supply are attached to the exposed portions of the wire and the resistive film.

The resistance of the graphite film can be tailored via its thickness. Alternatively, the film can be made from an electrically conductive paint, other than a colloidal graphite emulsion, chosen to impart the desired resistance. Yet another alternative is to tailor the resistance of a graphite film by exploiting the fact that its resistance can be changed permanently within about 10 percent by heating it to a temperature above 300 °C. Figure 2 depicts a coaxial heater, with electrical leads attached, that has been bent into an almost full circle for edge heating of a circular window. (In the specific application, there is a requirement for a heated cell window, through which an optical beam enters the cell.)

*This work was done by Dmitry Strekalov, Andrey Matsko, Anatoliy Savchenkov, and Lute Maleki of Caltech for NASA's Jet Propulsion Laboratory. Further information is contained in a TSP (see page 1).*
NPO-43569

# Dual-Input AND Gate From Single-Channel Thin-Film FET

**These transistors show potential as large-area, low-cost electronic circuitry on rigid and flexible substrates.**

*John H. Glenn Research Center, Cleveland, Ohio*

A regio-regular poly(3-hexylthiophene) (RRP3HT) thin-film transistor having a split-gate architecture has been fabricated on a doped silicon/silicon nitride substrate and characterized. RRP3HT is a semiconducting polymer that has a carrier mobility and on/off ratio when used in a field effect transistor (FET) configuration. This commercially available polymer is very soluble in common organic solvents and is easily processed to form uniform thin films. The most important polymer-based device fabricated and studied is the FET, since it forms the building block in logic circuits and switches for active matrix (light-emitting-diode) (LED) displays, smart cards, and radio frequency identification (RFID) cards.

Figure 1(a) shows a schematic cross-sectional view of the basic FET using an insulating gate dielectric layer over a doped silicon substrate. Two metal leads patterned over the insulator serve as the source and drain terminals of the device while the doped silicon serves as the global gate electrode. In this basic configuration, the gate voltage is applied to the bottom side of the wafer. To complete the FET, an organic semiconducting channel is placed between the source and drain terminals either via electrochemical deposition, vacuum deposition, or spin coating of the semiconductor material, resulting in a two-dimensional thin-film morphology; or via electrospinning, resulting in a one-dimensional nanofibrous morphology. In the dual-input architecture shown in Figure 1(b), metal contacts are located beneath the gate dielectric, and are accessed from the top side of the wafer by vias etched into the gate dielectric and semiconducting layers. Each gate contact serves as a device input, thus allowing for the design of various types of logic gates.

The dual-input device demonstrates AND logic functionality (see Figure 2),



(a)

**SCHEMATIC CROSS SECTIONAL VIEW OF A GLOBAL GATE FIELD EFFECT TRANSISTOR**

(b)

**SCHEMATIC CROSS SECTIONAL VIEW OF A SPLIT GATE FIELD EFFECT TRANSISTOR**

■ Semiconductor
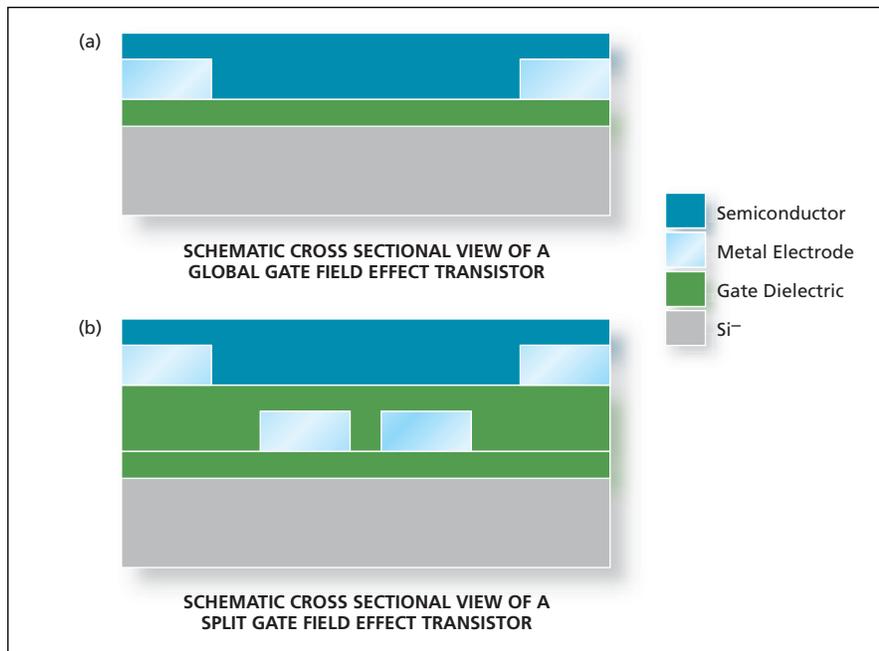■ Metal Electrode
■ Gate Dielectric
■ Si⁻

Figure 1. This cross-sectional view of the **Basic FET** shows (a) the global gate FET and (b) split-gate FET.
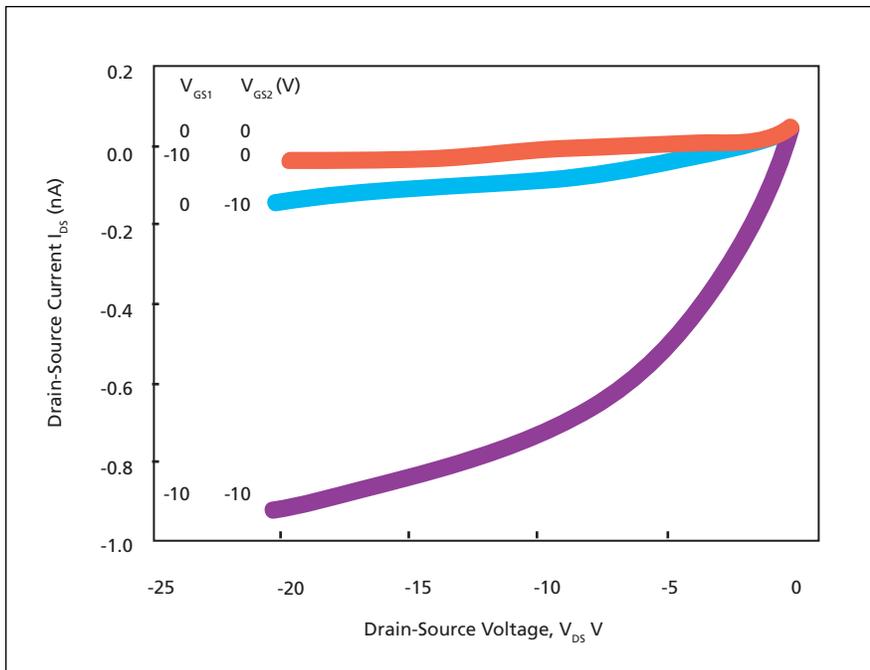
Figure 2. **Drain-Source Current vs Drain–Source Voltage Characteristics** are shown for the split gate field-effect transistor at different gate-source voltages.

and is controlled by applying either 0 or –10 volts to each of the gate electrodes. When –10 volts are simultaneously applied to both gates, the transistor is conductive (ON), while any other combination of gate voltages renders the transistor highly resistive (OFF). The p-type carrier charge mobility is about $5 \times 10^{-4} cm^2/V\text{-}s$. The low mobility is attributed to the sharp contours of the RRP3HT film between the drain and the source contacts, and to defects in the RRP3HT film itself.

The device substrates are fabricated with a starting wafer that is n-type doped Si (10 ohm-cm), with a 200-nm thick, ther-mally grown oxide layer. First, the gate metals, comprising 20-nm Cr/100-nm Au, are vacuum deposited in a thermal evaporator and patterned using conventional photolithographic and liftoff techniques. Next, a 100-nm-thick silicon nitride $(Si_3N_4)$ film is deposited over this using chemical vapor deposition (CVD). Access to the gate metallization is obtained by etching windows into the silicon nitride. The source and drain metallization, comprising 20-nm Cr/100-nm Au, is deposited on the CVD-grown silicon nitride on either side of the buried split gates using conventional photolithographic and liftoff techniques. The electrode "fingers" are about 20 microns wide and 600 microns long. The spacing between the electrodes is approximately 4 microns.

The split-gate architecture for logic circuitry is demonstrated via a two-input logic AND circuit. To create the device, a 10-Megohm load resistor is connected between the ground and the transistor source terminals, with the two gate terminals serving as the inputs. The output $(V_R)$ is taken at the source terminal across the load resistor. A low frequency ( 0.01 Hz) square-wave signal serves as the input gate bias. For all combinations of $V_{GS1}$ and $V_{GS2}$, except $V_{GS1} = V_{GS2} = -10$ V, the transistor is in the resistive "OFF" state, and $-0.3$ mV $< V_R < 0$ V. For $V_{GS1} = V_{GS2} - 10$ V, the transistor is in the more conductive "ON" state, causing a greater portion of the voltage drop to occur across the load resistor. As a result, $V_R$ is a more negative value ($-1.8$ mV $< V_R < -1.7$ mV).

When the device functions as an AND logic circuit, $V_{GS1}$ and $V_{GS2}$ are functions of time, while corresponding change in the output of voltage $V_R$ is a function of time for the four possible combinations of $V_{GS1}$ and $V_{GS2} = 0$ or $-10$ V. Larger outputs are observed only when both gates are simultaneously biased "high."

# High-Density, High-Bandwidth, Multilevel Holographic Memory
**Multiple terabytes could be read or written at a multigigahertz rate.**

*NASA's Jet Propulsion Laboratory, Pasadena, California*

A proposed holographic memory system would be capable of storing data at unprecedentedly high density, and its data-transfer performance in both reading and writing would be characterized by exceptionally high bandwidth. The capabilities of the proposed system would greatly exceed even those of a state-of-the art memory system, based on binary holograms (in which each pixel value represents 0 or 1), that can hold ≈1 terabyte of data and can support a reading or writing rate as high as 1 Gb/s.

The storage capacity of the state-of-the-art system cannot be increased without also increasing the volume and mass of the system. However, in principle, the storage capacity could be increased greatly, without significantly increasing the volume and mass, if multilevel holograms were used instead of binary holograms. For example, a 3-bit (8-level) hologram could store 8 terabytes, or an 8-bit (256-level) hologram could store 256 terabytes, in a system having little or no more size and mass than does the state-of-the-art 1-terabyte binary holographic memory.

The proposed system would utilize multilevel holograms. The system (see figure) would include lasers, imaging lenses and other beam-forming optics, a block photorefractive crystal wherein the holograms would be formed, and two multilevel spatial light modulators in the form of commercially available deformable-mirror-device spatial light modulators (DMDSLMs) made for use

in high-speed input conversion of data up to 12 bits. For readout, the system would also include two arrays of complementary metal oxide/semiconductor (CMOS) photodetectors matching the spatial light modulators. The system would further include a reference-beam-steering device (equivalent of a scanning mirror), containing no sliding parts, that could be either a liquid-crystal phased-array device or a microscopic mirror actuated by a high-speed micro-electromechanical system. Time-multiplexing and the multilevel nature of the DMDSLM would be exploited to enable writing and reading of multilevel holograms. The DMDSLM would also enable transfer of data at a rate of 7.6 Gb/s or perhaps somewhat higher.

**Multilevel Holograms** would be written to, and read from, the photorefractive crystal in this holographic memory system.

# Fabrication of Gate-Electrode Integrated Carbon-Nanotube Bundle Field Emitters

**Emission tips and a gate electrode are integrated into a monolithic device.**

*NASA's Jet Propulsion Laboratory, Pasadena, California*

A continuing effort to develop carbon-nanotube-based field emitters (cold cathodes) as high-current-density electron sources has yielded an optimized device design and a fabrication scheme to implement the design. One major element of the device design is to use a planar array of bundles of carbon nanotubes as the field-emission tips and to optimize the critical dimensions of the array (principally, heights of bundles and distances between them) to obtain high area-averaged current density and high reliability over a long operational lifetime — a concept that was discussed in more detail in "Arrays of Bundles of Carbon Nanotubes as Field Emitters" (NPO-40817), *NASA Tech Briefs*, Vol. 31, No. 2 (February 2007), page 58. Another major element of the design is to configure the gate electrodes (anodes used to extract, accelerate, and/or focus electrons) as a ring that overhangs a recess wherein the bundles of nanotubes are located [see Figure 1(a)], such that by virtue of the proximity between the ring and the bundles, a relatively low applied potential suffices to generate the large electric field needed for emission of electrons.

A fabrication process to monolithically integrate multiple electrodes is as follows. The starting workpiece is a commercially available double silicon-on-insulator (SOI) wafer comprising, from top layer to the bottom, a silicon device layer (1), a silicon dioxide (buried oxide) layer (2), another silicon device layer (3) on top of a silicon dioxide (buried oxide) layer (4), and a thick silicon substrate (bottom) layer (5). A schematic representation of the starting substrate is shown in Figure 2(a). After lithographic patterning followed by a combination of wet etching, deep reactive-ion etching (DRIE) and isotropic silicon etch by xenon difluoride ($XeF_2$) gas, overhanging gate and undercutting recess profiles are defined in the substrate. The iron catalytic dots are prepared at the bottom surface of the hole and carbon nanotube bundles are grown from them. Figures 1(a) shows a 3-D sketch and (b) shows an SEM micro-
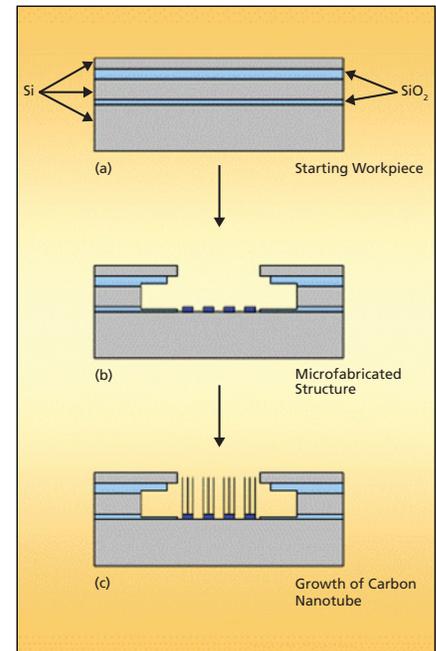


Figure 2. These are **Simplified Cross Sections** (not to scale) of the device of Figure 1 at various stages of fabrication.
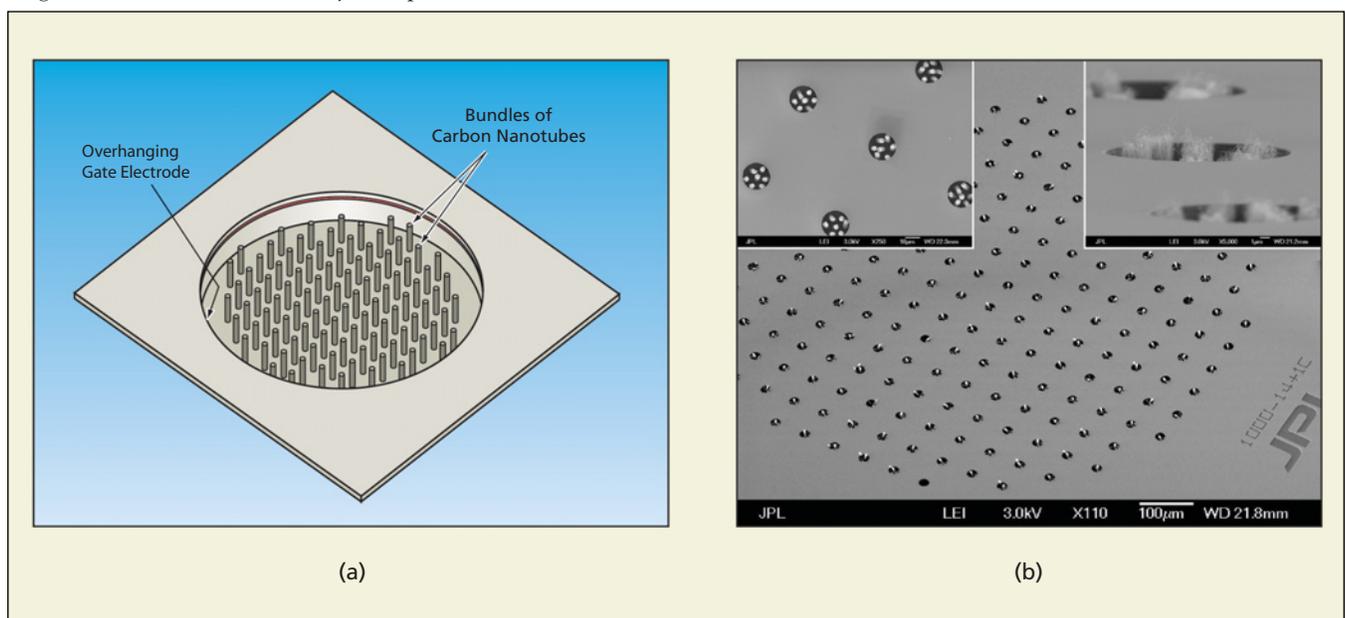


Figure 1. A **Gate Electrode Overhangs** a recess containing an array of bundles of carbon nanotubes (see part a). In part (b) are scanning electron micrograph (SEM) images of fabricated field-emitter devices.

graph of a completed device. In a completed device, the layer (1) acts as the gate electrode and layer (3) provides the mechanical support to achieve overhanging. However, layer (3) can also be used as an additional electrode for beam tailoring if required. Similarly, by using multiple-silicon-layer SOI substrates, monolithic integration of multiple electrodes can be achieved.

# Hydroxide-Assisted Bonding of Ultra-Low-Expansion Glass

**Preparation of bond surfaces is critical to success.**

*NASA's Jet Propulsion Laboratory, Pasadena, California*

A process for hydroxide-assisted bonding has been developed as a means of joining optical components made of ultra-low-expansion (ULE) glass, while maintaining sufficiently precise alignment between. The process is intended mainly for use in applications in which (1) bonding of glass optical components by use of epoxy does not enable attainment of the required accuracy and dimensional stability and (2) conventional optical contacting (which affords the required accuracy and stability) does not afford adequate bond strength.

The basic concept of hydroxide-assisted bonding is not new. The development of the present process was prompted by two considerations: (1) The expertise in hydroxide-assisted bonding has resided in very few places and the experts have not been willing to reveal the details of their processes and (2) data on the reliability and strength attainable by hydroxide-assisted bonding have been scarce.
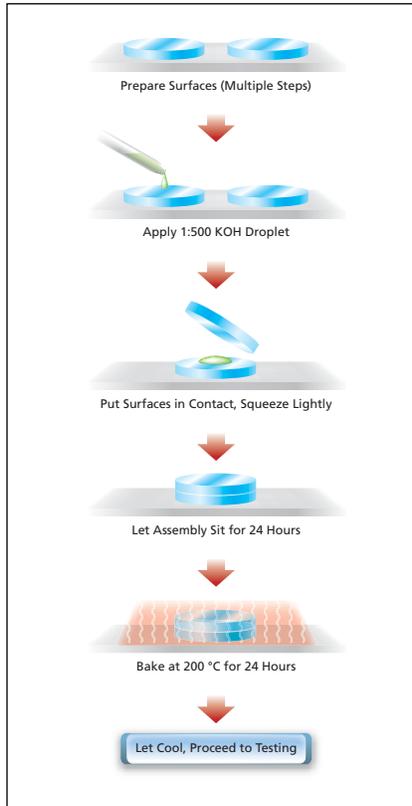
The first and most critical phase of the present hydroxide-assisted-bonding process is the preparation of the surfaces to be bonded. This phase includes the following steps:

2. Ultrasonic cleaning in successive baths of acetone, methanol, and propanol, using an ultrasound



**Two Prepared Surfaces** are placed in contact with a small amount of a hydroxide solution at the interface. The assembly is allowed to sit and is then baked. The resulting bond is at least as strong as an epoxy bond.

cleaner that operates at several Megahertz (Megasonics).

3. Treatment in a solution of potassium hydroxide and ammonium hydroxide in an ultrasonic cleaner, at Megahertz frequencies.

Thorough rinsing with deionized water is carried out after each of the above-mentioned steps. The last rinse is followed by ultrasonic cleaning in deionized water, then the cleaned surfaces are blow-dried with ionized air.

After preparation of the surfaces as described above, a droplet of a dilute solution of potassium hydroxide is placed on one of the surfaces, then the surfaces are placed in contact and gently squeezed together (see figure). The resulting assembly is allowed to sit at room temperature for 24 hours, and is then baked at a temperature of 200 °C for 24 hours.

In mechanical tests, sample bonds made by this process were found to have tensile strengths of at least 1.3 kpsi (≈9 MPa), where the epoxy bond used to attach the sample to the tensile stress test apparatus broke.

*This work was done by Alexander Abramovici and Victor White of Caltech for NASA's Jet Propulsion Laboratory. For more information, contact iaoffice@jpl.nasa.gov. NPO-45247*

# Photochemically Synthesized Polyimides

**Single monomers are polymerized by exposure to ultraviolet light, without heating.**

*John H. Glenn Research Center, Cleveland, Ohio*

An alternative to the conventional approach to synthesis of polyimides involves the use of single monomers that are amenable to photopolymerization. Heretofore, the synthesis of polyimides has involved multiple-monomer formulations and heating to temperatures that often exceed 250 °C. The present alternative approach enables synthesis under relatively mild conditions that can include room temperature.

The main disadvantages of the conventional approach are the following:

• Elevated production temperatures can lead to high production costs and can impart thermal stresses to the final products.

• If the proportions of the multiple monomeric ingredients in a given batch are not exactly correct, the molecular weight and other physical properties of the final material could be reduced

from their optimum or desired values.

To be useful in the alternative approach, a monomer must have a molecular structure tailored to exploit Diels-Alder trapping of a photochemically generated *ortho*-quinodimethane. (In a Diels-Alder reaction, a diene combines with a dienophile to form molecules that contain six-membered rings.) In particular, a suitable monomer (see figure) contains *ortho*-methylbenzophenone con-
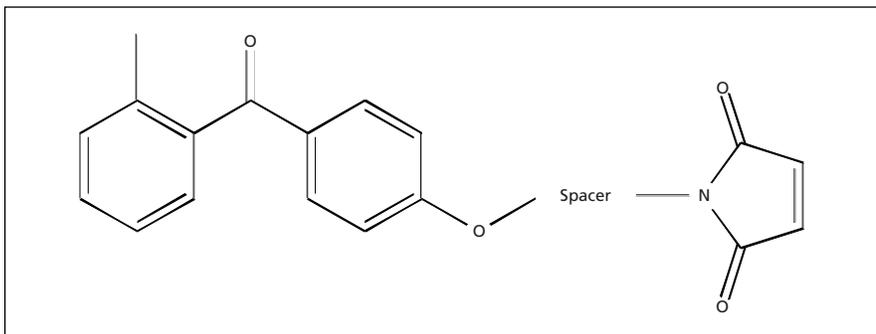
A **Monomer Molecule** suitable for photopolymerization contains a generic spacer group between an *ortho*-methylbenzophenone and a maleimide group.

nected to a dienophile (in this case, a maleimide) through a generic spacer group. Irradiation with ultraviolet light gives rise to a photochemical intermediate — the aforementioned *ortho*-quinodimethane — from the *ortho*-methylbenzophenone. This group may react with the dienophile on another such monomer molecule to produce an oligomer that, in turn may react in a step-growth manner to produce a polyimide.

This approach offers several advantages in addition to those mentioned above:
• The monomer can be stored for a long time because it remains unreactive until exposed to light.
• Because the monomer is the only active starting ingredient, there is no need for mixing, no concern for ensuring correct proportions of monomers, and the purity of the final product material is inherently high.
• The use of solvents is optional: The synthesis can be performed using the neat monomer or the monomer mixed with one or more solvent(s) in dilute or concentrated solution.
• The solubility of the monomer and the physical and chemical properties of the final polymer can be tailored through selection of the spacer group.

*This work was done by Michael A. Meador of Glenn Research Center and Daniel S. Tyson and Faysal Ilhan of Ohio Aerospace Institute. Further information is contained in a TSP (see page 1).*

*Inquiries concerning rights for the commercial use of this invention should be addressed to NASA Glenn Research Center, Innovative Partnerships Office, Attn: Steve Fedor, Mail Stop 4–8, 21000 Brookpark Road, Cleveland, Ohio 44135. Refer to LEW-18174-1.*

# Optimized Carbonate and Ester-Based Li-Ion Electrolytes

**This technology can be used in portable electronics, cell phones, and electric vehicles.**

*NASA's Jet Propulsion Laboratory, Pasadena, California*

To maintain high conductivity in low temperatures, electrolyte co-solvents have been designed to have a high dielectric constant, low viscosity, adequate coordination behavior, and appropriate liquid ranges and salt solubilities. Electrolytes that contain ester-based co-solvents in large proportion (>50 percent) and ethylene carbonate (EC) in small proportion (<20 percent) improve low-temperature performance in MCMB carbon-$LiNiCoO_2$ lithium-ion cells. These co-solvents have been demonstrated to enhance performance, especially at temperatures down to –70 ºC. Low-viscosity, ester-based co-solvents were incorporated into multi-component electrolytes of the following composition: 1.0 M $LiPF_6$ in ethylene carbonate (EC) + ethyl methyl carbonate (EMC) + X (1:1:8 volume percent) [where X = methyl butyrate (MB), ethyl butyrate EB, methyl propionate (MP), or ethyl valerate (EV)]. These electrolyte formulations result in improved low-temperature performance of lithium-ion cells, with dramatic results at temperatures below –40 ºC. [See "Ester-Based Electrolytes for Low-Temperature Li-Ion Cells," (NPO-41097) *NASA Tech Briefs*, Vol 29, No. 12 (December, 2005), p. 59.]

Improved low-temperature performance can also be realized with ester-based electrolytes containing high salt concentrations and by using mixed salt formulations — specifically with (a) 1.0 M $LiPF_6$ + 0.40 $LiBF_4$ and (b) 1.40 M $LiPF_6$ dissolved in EC+EMC+MP (1:1:8 volume percent) and EC+EMC+MB (1:1:8 volume percent) solvent mixtures. The rate capability has been observed to increase dramatically at low temperatures (i.e., –60 ºC) using this approach. It is anticipated that increased salt concentrations and the use of mixed salt systems will also improve the low-temperature performance characteristics of other solvent blends of carbonates and esters. ["Mixed-Salt/Ester Electrolytes for Low-Temperature Li + Cells" (NPO-42862), *NASA Tech Briefs*, Vol. 30, No. 11 (November 2006), p 66.]

A number of these electrolytes have been demonstrated in both experimental and aerospace-quality, high-capacity prototype cells. In more recent work, these ester-containing electrolytes have been further optimized to provide both good low-temperature performance (down to –60 ºC) while still offering reasonable high-temperature resilience. This has primarily been achieved by fixing the EC-content at 20 percent and the ester co-solvent at 20 percent, in contrast to the previously developed ultra-low temperature systems, which have the EC-content and ester-content at 10 percent and 80 percent, respectively. Using this approach, a prototype cell containing a 1.0 M $LiPF_6$ EC+EMC+MP (20:60:20 volume percent) electrolyte was capable of delivering over six times the amount of capacity delivered by the baseline ternary, all-carbonate blend, and was able to support reasonably aggressive rates at low temperature (–50 and –60 ºC). Cells containing other esters also performed well at low temperature, with the lower-molecular-weight, lower-viscosity co-solvents generally yielding better performance at low temperatures.

Although slightly less favorable in terms of electrolyte conductivity, the higher-molecular-weight esters [i.e., propyl butyrate (PB), and butyl butyrate (BB)] are expected to result in cells with more favorable high-temperature resilience (>40 ºC), compared to the lower-molecular-weight esters.

This technology has relevance for manned and unmanned space missions, aircraft batteries, and Land Warrior applications, as well as for terrestrial applica-

tions that require good performance and a high level of safety over a range of temperatures, including portable electronics like camcorders, cellular phones, laptop computers, and radio communication sets. Electric vehicle applications can also use this innovation where high-power batteries must operate at low temperatures, such as in monitoring stations in Antarctica.

# Compact 6-DOF Stage for Optical Adjustments
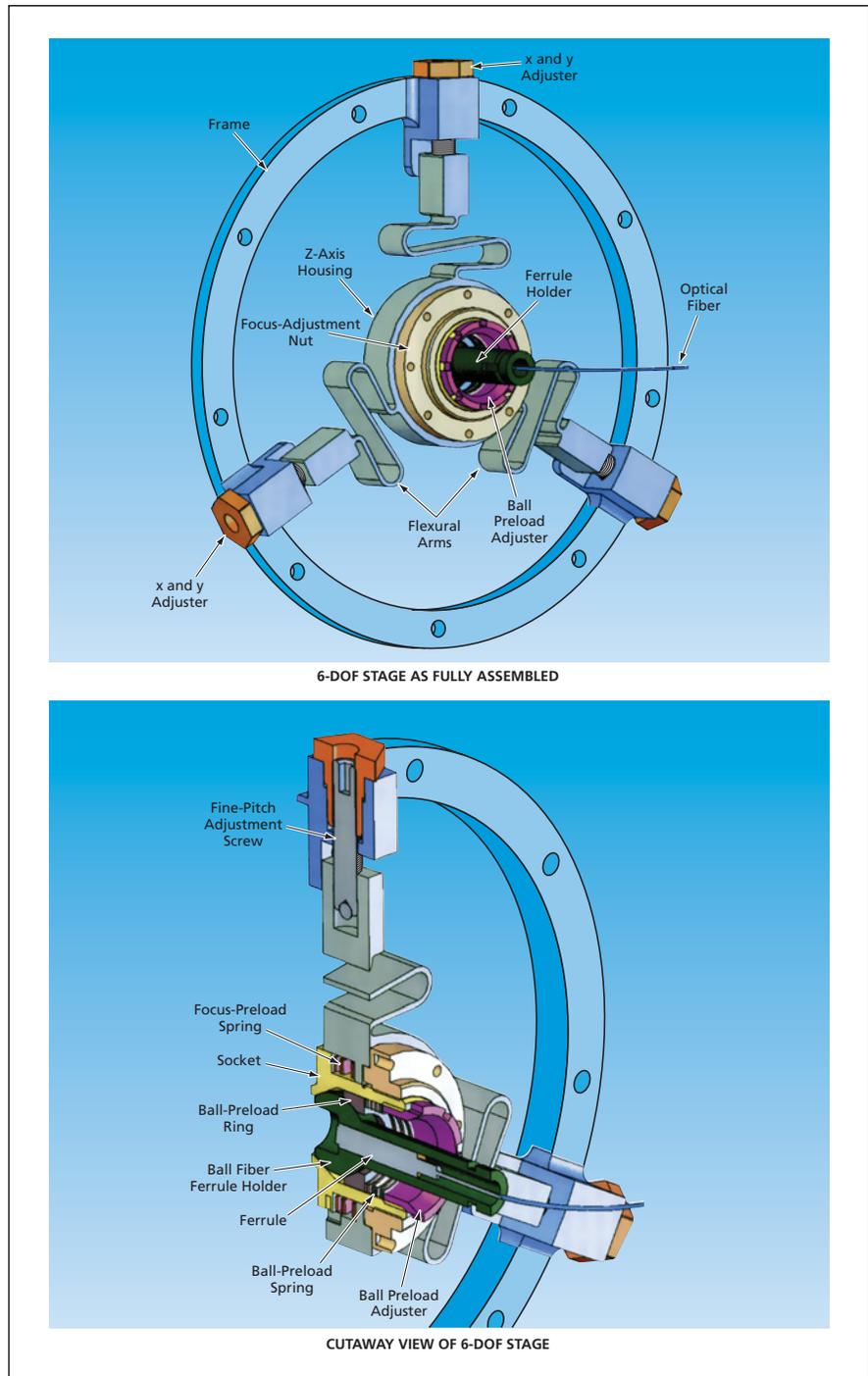**Adjustments can be made in all translational and rotational degrees of freedom.**

*NASA's Jet Propulsion Laboratory, Pasadena, California*

The figure depicts selected aspects of a six-degree-of-freedom (6-DOF) stage for mechanical adjustment of an optical component. The six degrees of freedom are translations along the Cartesian axes ($x$, $y$, and $z$) and rotations about these axes ($\theta_x$, $\theta_y$, and $\theta_z$, respectively). Relative to prior such stages, this stage offers advantages of compactness, stability, and robustness, plus other advantages as described below.

The stage was designed specifically as part of a laser velocimeter and altimeter in which light reflected by a distant object is collected by a Cassegrainian telescope and focused into a single-mode, polarization-maintaining optical fiber. The stage is used to position and orient the input end of the optical fiber with respect to the focal point of the telescope. Stages like this one can also be adapted for use in positioning and orienting other optical components, including lenses, prisms, apertures, and photodetectors.

The optical fiber or other optical component is mounted in a ferrule that is, in turn, mounted in a ferrule holder that is an extension of the ball part of a ball-and-socket assembly that enables adjustment in all three rotational degrees of freedom. The position of the ferrule within the ferrule holder is set so that the center of the input face of the optical component lies at the center of the ball. As a result of this setting, rotational adjustment is not accompanied by undesired translational adjustment.

The subassembly comprising the ball, ferrule holder, and optical component is spring-loaded into the socket, and the spring load can be adjusted by means of a threaded ball-preload adjuster. The ferrule holder and the ball-preload adjuster are equipped with external surfaces that mate with special-purpose adjustment tools. The spring load is chosen to make the frictional torque between the ball and the socket small enough that rotational adjustments can be made, yet large enough that the ball and socket retain their relative angular position once the angular adjustment



**6-DOF STAGE AS FULLY ASSEMBLED**



**CUTAWAY VIEW OF 6-DOF STAGE**

This **Compact Assembly** enables stable adjustment of the input end of the optical fiber in all three translational and all three rotational degrees of freedom. Rotational adjustments can be made without causing undesired translations, and translational adjustments can be made without causing undesired rotations.

has been completed and the rotational-adjustment tools removed.

Optionally, the ball-and-socket assembly as described thus far could be used alone as a rotation-only stage. However, in the original application, the ball-and-socket assembly is mounted within a z-axis housing that, as its name suggests, enables translational adjustment along the z axis (focus adjustment). The socket is in threaded engagement with a focus-adjustment nut that can be turned about the z axis to make the adjustment. An anti-rotation pin that is free to translate along a z-oriented slot prevents undesired rotation of the socket about the z axis during focus adjustment. A focus-preload spring exerts a z-axis preload between the socket and the z-axis housing to prevent backlash in the focus adjustment.

Optionally, the z-axis-adjusting mechanism as described above could be used alone as a z-axis-translation stage. However, in the original application, it is mounted in an x–y translation stage that includes three flexural arms positioned at equal angular intervals on a circular frame. The radial position of the outer end of each flexural arm can be varied by means of a fine-pitch adjustment screw. Initially, all three adjustment screws are set at approximately the midpoints of their ranges, thereby placing all three flexural arms in tension and ap-proximately centering the z-axis housing in the circle. Thereafter, the screws are turned, singly or in pairs as needed, to make fine adjustments to bring the optical component into x and y alignment. Care must be taken during these adjustments to maintain all three flexural arms in tension so as to prevent backlash. The x–y adjustment resolution is much finer than the thread pitch of the adjustment screws. Optionally, like the rotational and z-axis sub-stages, the x–y stage could be used by itself.

# Ultrasonic/Sonic Impacting Penetrators
## Soil can be probed relatively gently to a depth of several feet.

*NASA's Jet Propulsion Laboratory, Pasadena, California*

Ultrasonic/sonic impacting penetrators (USIPs) are recent additions to the series of apparatuses based on ultrasonic/sonic drill corers (USDCs). A USIP enables a rod probe to penetrate packed soil or another substance of similar consistency, without need to apply a large axial force that could result in buckling of the probe or in damage to some buried objects. USIPs were conceived for use in probing and analyzing soil to depths of tens of centimeters in the vicinity of buried barrels containing toxic waste, without causing rupture of the barrels. USIPs could also be used for other purposes, including, for example, searching for pipes, barrels, or other hard objects buried in soil; and detecting land mines.

USDCs and other apparatuses based on USDCs have been described in numerous previous *NASA Tech Briefs* articles. The ones reported previously were designed, variously, for boring into, and/or acquiring samples of, rock or other hard, brittle materials of geological interest. To recapitulate: A USDC can be characterized as a lightweight, low-power, piezoelectrically driven jackhammer in which ultrasonic and sonic vibrations are generated and coupled to a tool bit. As shown in the figure, a basic USDC includes a piezoelectric stack, a backing and a horn connected to the stack, a free mass ("free" in the sense that it can slide axially a short distance between the horn and the shoulder of tool bit), and a tool bit, i.e., probe for USIP. The piezoelectric stack is driven at the resonance frequency of the stack/horn/backing assembly to create ultrasonic vibrations that are mechanically amplified by the horn. To prevent fracture during operation, the piezoelectric stack is held in compres-sion by a bolt. The bouncing of the free mass between the horn and the tool bit at sonic frequencies generates hammering actions to the bit that are more effective for drilling than is the micro-hammering action of ultrasonic vibrations in ordinary ultrasonic drills. The hammering actions are so effective that the axial force needed to make the tool bit advance into the material of interest is much smaller than in ordinary twist drilling, ultrasonic drilling, or ordinary steady pushing.

The differences between a USIP and a USDC-based apparatus described above lie in design details that make a USIP more suitable for penetrating packed soil. The piezoelectric stack in an experimental prototype USIP had a diameter of 1.0 in. (≈25 mm) and could be made to resonate at a frequency between 12 and 20 kHz, the exact value depending on the
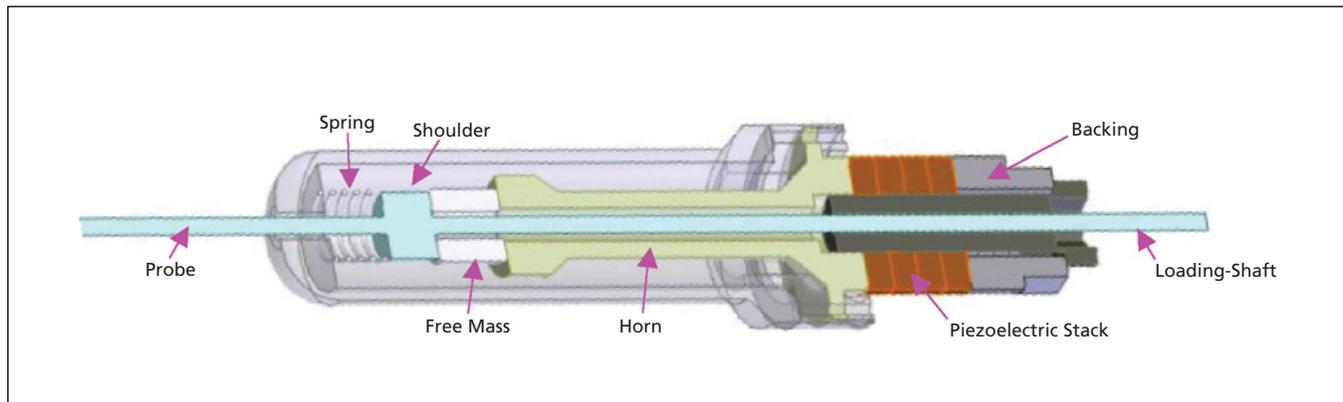


The design of **Prototype USIP** shows key components.

specific design and operating conditions. The probe rod had a diameter of 1/8 in. (≈3 mm) and a length sufficient to enable penetration to a depth of 3 ft (≈91 cm). The piezoelectric stack was driven at a 20-percent duty cycle, with a combination of automatic and manual adjustments of the frequency of the driving signal to compensate for changes in the resonance frequency induced by changes in mechanical loading and by temperature rise during operation.

The design of the horn and a piezoelectric-stack-backing structure was optimized for coupling power from the stack to the horn and for amplification of the longitudinal displacement. The optimization was accomplished with the help of a computer program that numerically solved the governing equations to perform impact and vibration-mode analyses. The modal analysis was used to determine the dimensions of the horn and backing for a resonance frequency in the required range and to further adjust the dimensions of the horn so that the neutral plane matched the mounting plane to minimize adverse effects of transducer vibration on a supporting structure. The impact analysis, in which the focus was on the interaction between the free mass and the horn, was used to derive an optimal weight of the free mass.

In experiments, an axial force of 7 lb (≈31 N)] was found to be sufficient to cause the probe tip to reach a depth of 3 ft (≈91 cm) in a packed soil sample. In contrast, the axial force that would be needed to make an equivalent probe tip penetrate to the same depth by ordinary steady pushing has been estimated to be about 200 lb (≈890 N), which is large enough to easily cause buckling of the probe without a holding mechanism and to damage a buried barrel.

# Miniature, Lightweight, One-Time-Opening Valve
## A small solder plug is melted to release a pressurized gas.

*NASA's Jet Propulsion Laboratory, Pasadena, California*

The figure depicts the main parts of a prototype miniature, lightweight, one-time-opening valve. Like some other miniature one-time-opening valves reported in previous issues of *NASA Tech Briefs*, this valve is opened by melting a material that blocks the flow path. This valve is designed to remain closed at some temperature between room temperature and cryogenic temperature until the time of opening.

The prototype valve includes a 1/8-in. (3-mm) aluminum tube, one end of which is plugged with a solder comprising about 37 weight percent of lead and 63 weight percent of tin. The tube and the solder both have a coefficient of thermal expansion of 23 micron/m-K at room temperature. Before plugging, the interior surface of the plug end of the tube is cleaned with a commercial flux paste developed specifically for preparing aluminum for bonding with lead/tin solder. The solder is then melted into the cleaned end of the tube, forming the plug.

In a test, the plugged tube was pressurized to 1,000 psi (6.9 MPa) with he-



**SOLDERED ALUMINUM TUBE BEFORE HEATING**

**SOLDERED ALUMINUM TUBE AFTER HEATING**

The **Solder Plug Was Ejected** from the pressurized aluminum tube when the plugged end was heated to about 200 °C.

lium and leak-tested. It was then cooled to a temperature of 77 K (about –196 °C) and again leak-tested at the same pressure. Finally, at a lower pressure, the plugged end of the tube was heated to about 200 °C (the melting temperature of the solder is 183°C), causing the solder plug to be ejected (see figure). It has been estimated that in a subsequent version of the valve, the plug could be melted by electrical heating, using a nichrome wire having a mass of only 10 g.

# Software

## Supplier Management System

Supplier Management System (SMS) allows for a consistent, agency-wide performance rating system for suppliers used by NASA. This version (2.0) combines separate databases into one central database that allows for the sharing of supplier data. Information extracted from the NBS/Oracle database can be used to generate ratings. Also, supplier ratings can now be generated in the areas of cost, product quality, delivery, and audit data. Supplier data can be charted based on real-time user input. Based on these individual ratings, an overall rating can be generated.

Data that normally would be stored in multiple databases, each requiring its own log-in, is now readily available and easily accessible with only one log-in required. Additionally, the database can accommodate the storage and display of quality-related data that can be analyzed and used in the supplier procurement decision-making process. Moreover, the software allows for a Closed-Loop System (supplier feedback), as well as the capability to communicate with other federal agencies.

While Version 1.0 only had an Approved Supplier list, Version 2.0 includes the Approved Supplier List, Supplier Rating System, and the Supplier Outreach and Process Control Assurance System. The Supplier Rating System is a new database that was developed specifically for this software. The system allows for segregation of data to ensure sensitive data is protected.

*This program was written by Eric Ramirez, Sandy Gutheinz, James Brison, Anita Ho, James Allen, Olga Ceritelli, Claudia Tobar, Thuykien Nguyen, and Harrel Crenshaw of Caltech and Roxann Santos of SkillStorm Inc. for NASA's Jet Propulsion Laboratory.*

*This software is available for commercial licensing. Please contact Karina Edmonds of the California Institute of Technology at (626) 395-2322. Refer to NPO-44084.*

## Improved CLARAty Functional-Layer/Decision-Layer Interface

Improved interface software for communication between the CLARAty Decision and Functional layers has been developed. [The Coupled Layer Architecture for Robotics Autonomy (CLARAty) was described in "Coupled-Layer Robotics Architecture for Autonomy" (NPO-21218), *NASA Tech Briefs*, Vol. 26, No. 12 (December 2002), page 48. To recapitulate: the CLARAty architecture was developed to improve the modularity of robotic software while tightening coupling between planning/execution and basic control subsystems. Whereas prior robotic software architectures typically contained three layers, the CLARAty contains two layers: a decision layer (DL) and a functional layer (FL).] Types of communication supported by the present software include sending commands from DL modules to FL modules and sending data updates from FL modules to DL modules.

The present software supplants prior interface software that had little error-checking capability, supported data parameters in string form only, supported commanding at only one level of the FL, and supported only limited updates of the state of the robot. The present software offers strong error checking, and supports complex data structures and commanding at multiple levels of the FL, and relative to the prior software, offers a much wider spectrum of state-update capabilities.

*This program was written by Tara Estlin, Gregg Rabideau, Daniel Gaines, Mark Johnston, Caroline Chouinard, Issa Nessnas, and I-Hsiang Shu of Caltech for NASA's Jet Propulsion Laboratory. Further information is contained in a TSP (see page 1).*

*This software is available for commercial licensing. Please contact Karina Edmonds of the California Institute of Technology at (626) 395-2322. Refer to NPO-44571.*

## JAVA Stereo Display Toolkit

This toolkit provides a common interface for displaying graphical user interface (GUI) components in stereo using either specialized stereo display hardware (e.g., liquid crystal shutter or polarized glasses) or anaglyph display (red/blue glasses) on standard workstation displays. An application using this toolkit will work without modification in either environment, allowing stereo software to reach a wider audience without sacrificing high-quality display on dedicated hardware.

The toolkit is written in Java for use with the Swing GUI Toolkit and has cross-platform compatibility. It hooks into the graphics system, allowing any standard Swing component to be displayed in stereo. It uses the OpenGL graphics library to control the stereo hardware and to perform the rendering. It also supports anaglyph and special stereo hardware using the same API (application-program interface), and has the ability to "simulate" color stereo in anaglyph mode by combining the red band of the left image with the green/blue bands of the right image.

This is a low-level toolkit that accomplishes simply the display of components (including the JadeDisplay image display component). It does not include higher-level functions such as disparity adjustment, 3D cursor, or overlays — all of which can be built using this toolkit.

*This program was written by Robert Deen and Oleg Pariser of Caltech for NASA's Jet Propulsion Laboratory.*

*The software used in this innovation is available for commercial licensing. Please contact Karina Edmonds of the California Institute of Technology at (626) 395-2322. Refer to NPO-43786.*

## Remote-Sensing Time Series Analysis, a Vegetation Monitoring Tool

The Time Series Product Tool (TSPT) is software, developed in MATLAB®, which creates and displays high signal-to-noise Vegetation Indices imagery and other higher-level products derived from remotely sensed data. This tool enables automated, rapid, large-scale regional surveillance of crops, forests, and other vegetation. TSPT temporally processes high-revisit-rate satellite imagery produced by the Moderate Resolution Imaging Spectroradiometer (MODIS) and by other remote-sensing systems. Although MODIS imagery is acquired daily, cloudiness and other sources of noise can greatly reduce the effective temporal resolution. To improve cloud statistics, the TSPT combines MODIS data from multiple satellites (Aqua and Terra). The TSPT produces MODIS products as single time-frame and multitemporal change images, as time-series plots at a selected

location, or as temporally processed image videos. Using the TSPT program, MODIS metadata is used to remove and/or correct bad and suspect data. Bad pixel removal, multiple satellite data fusion, and temporal processing techniques create high-quality plots and animated image video sequences that depict changes in vegetation greenness. This tool provides several temporal processing options not found in other comparable imaging software tools. Because the framework to generate and use other algorithms is established, small modifications to this tool will enable the use of a large range of remotely sensed data types.

An effective remote-sensing crop-monitoring system must be able to detect subtle changes in plant health in the earliest stages, before the effects of a disease outbreak or other adverse environmental conditions can become widespread and devastating. The integration of the time series analysis tool with ground-based information, soil types, crop types, meteorological data, and crop growth models in a Geographic Information System, could provide the foundation for a large-area crop-surveillance system that could identify a variety of plant phenomena and improve monitoring capabilities.

*This program was written by Rodney McKellip of Stennis Space Center; Donald Prados of Computer Sciences Corporation; Robert Ryan, Kenton Ross, and Joseph Spruce of Science Systems and Applications; and Gerald Gasser and Randall Greer of Lockheed Martin Space Operations, Information Systems Directorate.*

*Inquiries concerning rights for the commercial use of this invention should be addressed to the Intellectual Property Manager at Stennis Space Center (228) 688-1929. Refer to SSC-00261, volume, and number of this* NASA Tech Briefs *issue and the page number.*

---

### ⟐ PyPele Rewritten To Use MPI

A computer program known as "PyPele," originally written as a Python-language extension module of a C++ language program, has been rewritten in pure Python language. The original version of PyPele dispatches and coordinates parallel-processing tasks on cluster computers and provides a conceptual framework for spacecraft-mission-design and -analysis software tools to run in an embarrassingly parallel mode. The original version of PyPele uses SSH (Secure Shell — a set of standards and an associated network protocol for establishing a secure channel between a local and a remote computer) to coordinate parallel processing. Instead of SSH, the present Python version of PyPele uses Message Passing Interface (MPI) [an unofficial *de-facto* standard language-independent application programming interface for message-passing on a parallel computer] while keeping the same user interface.

The use of MPI instead of SSH and the preservation of the original PyPele user interface make it possible for parallel application programs written previously for the original version of PyPele to run on MPI-based cluster computers. As a result, engineers using the previously written application programs can take advantage of embarrassing parallelism without need to rewrite those programs.

*This program was written by George Hockney and Seungwon Lee of Caltech for NASA's Jet Propulsion Laboratory.*

*This software is available for commercial licensing. Please contact Karina Edmonds of the California Institute of Technology at (626) 395-2322. Refer to NPO-44729.*

---

### ◎ Data Assimilation Cycling for Weather Analysis

This software package runs the atmospheric model MM5 in data assimilation cycling mode to produce an optimized weather analysis, including the ability to insert or adjust a hurricane vortex. The program runs MM5 through a cycle of short forecasts every three hours where the vortex is adjusted to match the observed hurricane location and storm intensity. This technique adjusts the surrounding environment so that the proper steering current and environmental shear are achieved. MM5cycle uses a Cressman analysis to blend observation into model fields to get a more accurate weather analysis. Quality control of observations is also done in every cycle to remove bad data that may contaminate the analysis. This technique can assimilate and propagate data in time from intermittent and infrequent observations while maintaining the atmospheric field in a dynamically balanced state.

The software consists of a C-shell script (MM5cycle.driver) and three FORTRAN programs (splitMM5files.F, comRegrid.F, and insert_vortex.F), and are contained in the pre-processor component of MM5 called "Regridder." The model is first initialized with data from a global model such as the Global Forecast System (GFS), which also provides lateral boundary conditions. These data are separated into single-time files using splitMM5.F. The hurricane vortex is then bogussed in the correct location and with the correct wind field using insert_vortex.F. The modified initial and boundary conditions are then recombined into the model fields using comRegrid.F. The model then makes a three-hour forecast. The three-hour forecast data from MM5 now become the analysis for the next short forecast run, where the vortex will again be adjusted. The process repeats itself until the desired time of analysis is achieved. This code can also assimilate observations if desired.

*This program was written by Nam Tran, Yongzuo Li, and Patrick Fitzpatrick of the GeoResources Institute at Mississippi State University for Stennis Space Center.*

*Inquiries concerning rights for its commercial use should be addressed to:*

*GeoResources Institute*
*Mississippi State University*
*Building 1103, Room 233*
*Stennis Space Center, MS 39529*
*Phone No.: (228) 688-4218*
*Web site: www.gri.msstate.edu*
*Refer to SSC-00276/7, the volume and number of this* NASA Tech Briefs *issue, and the page number.*

# Hydrocyclone/Filter for Concentrating Biomarkers From Soil

**This apparatus could detect biomarkers or chemical waste in soil.**

*NASA's Jet Propulsion Laboratory, Pasadena, California*

The hydrocyclone-filtration extractor (HFE), now undergoing development, is a simple, robust apparatus for processing large amounts of soil to extract trace amounts of microorganisms, soluble organic compounds, and other biomarkers from soil and to concentrate the extracts in amounts sufficient to enable such traditional assays as cell culturing, deoxyribonucleic acid (DNA) analysis, and isotope analysis. Originally intended for incorporation into a suite of instruments for detecting signs of life on Mars, the HFE could also be used on Earth for similar purposes, including detecting trace amounts of biomarkers or chemical wastes in soils.

In addition to a conical separator vessel typical of a hydrocyclone, the HFE includes a pump, a sample container, an electropositive nanoparticle filter, and associated plumbing (see figure). The hydrocyclone serves to separate both cellular-sized particles (<5 μm) and dissolved organic compounds from the bulk soil (consisting mostly of particles larger than 5 μm). The electropositive filter serves to capture cellular biomass and remove particles from the extract with maximal capacity (that is, minimal clogging).

The soil sample is prepared by mixing it with sterile water or another suitable solvent to form a slurry, which is pumped to the hydrocyclone separator vessel in tangential streams at the top (wide) end to form two concentric opposing vortices at high hydrodynamic pressures to effect separation based on particle size. The spinning motion of the injected slurry is accelerated by the conical taper, creating a large centrifugal force that causes the larger particles to rapidly separate from the rest of the flow and leave the vessel as part of underflow through the bottom (narrow) end of the separator vessel. The liquid containing suspended particles smaller than 5 μm leaves the vessel as the overflow (which is larger than the underflow) at the top (wide) end of the vessel. The overflow is then fed through the filter.
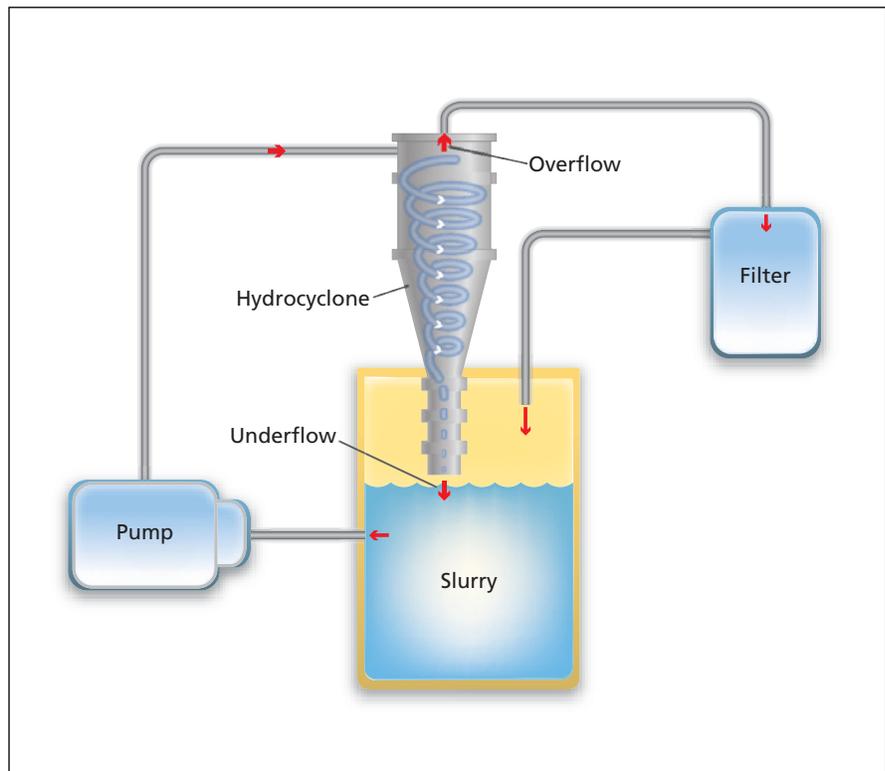


In this **Prototype HFE**, a soil/water slurry is pumped from a sample container through a hydrocyclone separator vessel and a filter and is recycled through the sample container. The hydrocyclone separates most of the soil particles into an underflow. The filter traps smaller particles in the overflow.

The filter contains electropositive aluminum nanotubes embedded in a glass-fiber matrix. The filter has a nominal pore size of 2 μm, but can collect biological particles having sizes down to fractions of a micron, on the basis of electrostatic charge, without clogging. The combination of the hydrocyclone and the electropositive nanoparticle filter is capable of extracting 99 percent of particles smaller than 5 μm from the soil sample and retaining them for analysis. In the prototype HFE depicted schematically in the filter, the underflow and the effluent from the filter are fed back to the sample container. It is envisioned that the fully developed HFE could operate in a continuous-flow mode, making it possible to extract biomarkers from a large volume (e.g., 1 m$^3$) of soil using a minimal amount (e.g., 1 L) of solvent.

In a field test, the prototype HFE was made to process a slurry consisting of 4 L of sterile water mixed with 4 L of Atacama-desert soil, which contains such low concentrations of recoverable microorganisms as to be nearly impossible to analyze in the absence of an extraction-and-concentration process. After 15 minutes of recycling the slurry in the HFE, the maximum loading of the filter was reached. The filter was removed and dried and found to contain 100 g of fine particulate material, which, in turn, was removed from the filter in a laboratory for further analysis. Whereas traditional extraction protocols yielded no microbial colony-forming units, the extract from the HFE filter yielded microbes too numerous to count on standard growth plates. On the basis of development plans and this result, it is expected that

cellular-extract concentrations obtained by use of the fully developed HFE will be at least $10^3$ times those obtained by means of state-of-the art extraction methods heretofore used in environmental microbiology.

*This work was done by Adrian Ponce of Caltech and Donald Obenhuber of National*

Research Council for NASA's Jet Propulsion Laboratory. Further information is contained in a TSP (see page 1).

*In accordance with Public Law 96-517, the contractor has elected to retain title to this invention. Inquiries concerning rights for its commercial use should be addressed to:*

*Innovative Technology Assets Management*

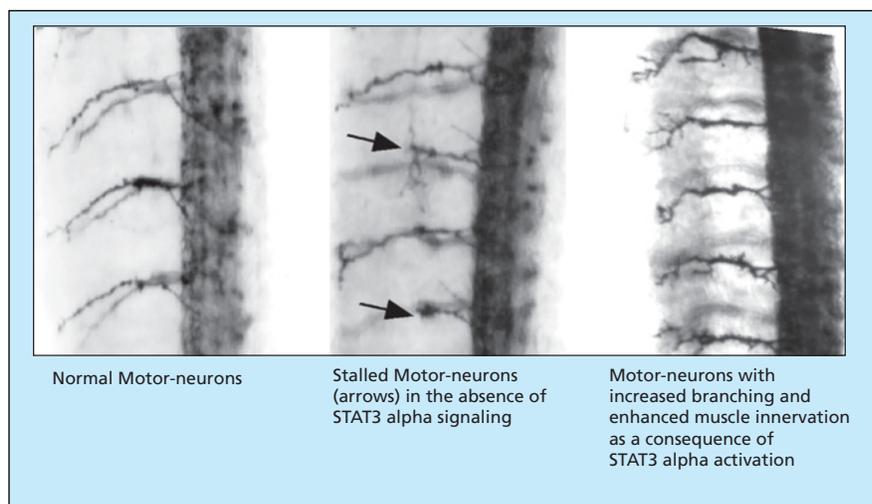# Activating STAT3 Alpha for Promoting Healing of Neurons

## Natural anti-apoptotic, pro-axogenic mechanisms are stimulated artificially.

*Ames Research Center, Moffett Field, California*

A method of promoting healing of injured or diseased neurons involves pharmacological activation of the STAT3 alpha protein. Usually, injured or diseased neurons heal incompletely or not at all for two reasons: (1) they are susceptible to apoptosis (cell death); and (2) they fail to engage in axogenesis — that is, they fail to re-extend their axons to their original targets (e.g., muscles or other neurons) because of insufficiency of compounds, denoted neurotrophic factors, needed to stimulate such extension. The present method (see figure) of treatment takes advantage of prior research findings to the effect that the STAT3 alpha protein has anti-apoptotic and pro-axogenic properties.

As used here, "STAT" signifies "signal transducer and activator of transcription." "STAT3 alpha" is the name of one of a number of transcription factors and of the gene responsible for producing it. Transcription factors activate the expression of other genes and otherwise generally regulate gene expression. The STAT3 alpha protein is activated in response to such extracellular factors as hormones and growth factors as well as the aforementioned neurotrophic factors. The STAT3 alpha protein associates with trans-membrane receptors for these extracellular factors. When activated by growth factors and hormones, STAT3 alpha prevents apoptosis.

Recent findings from the Life Sciences and Microgravity Division of Ames Research Center now show that when activated by neurotrophic factors STAT3 alpha, in addition to preventing apoptosis, also promotes innervation. The natural activation of the STAT3 alpha protein is effected by phosphorylation of a specific tyrosine amino acid. Upon such phosphorylation, two STAT3 alpha mol-



**Normal Motor-neurons**

**Stalled Motor-neurons (arrows) in the absence of STAT3 alpha signaling**

**Motor-neurons with increased branching and enhanced muscle innervation as a consequence of STAT3 alpha activation**

**Motor Neurons** visualized by a dark staining reaction are seen exiting the spinal cord, from the right side of each panel, innervating adjacent muscle tissue.

ecules can form a homo-dimer. The tyrosine on a given STAT3 protein molecule that becomes phosphorylated resides on a flexible activation loop sequence that binds to a pocket, denoted the SH2 domain, of another STAT3 protein molecule. Upon homo-dimerization, STAT3 alpha is retained in the nucleus of cells, where it binds specific deoxyribonucleic acid (DNA) sequences and activates the expression of nearby genes. Thus, homo-dimerized STAT3 alpha protein is part of a signal-transduction complex that relays chemical signals from hormones, growth factors, and neurotrophic factors outside the cell directly to the DNA inside the cell. In so doing, it activates genes that exert anti-apoptotic and axogenic effects.

Hence, the present method is based on the design of a new class of pharmacological agents (homo and heteroditopic Janus molecules) to promote artificial dimerization and pharmacological activa-

tion of therapeutic targets, in this case the STAT3 alpha protein. The precise location of each atom in the STAT3 homo-dimer is known and it is possible to use this structural information along with molecular modeling and docking programs to rationally design a Janus molecule having the correct sizes and shape, and/or to bind to STAT3 alpha preferentially to other proteins that are similar to STAT3 alpha. The compound can be synthesized by techniques that are well established in the pharmaceutical industry and can be formulated to be administered alone or in combination with other therapeutic compounds.

*This work was done by Greg Conway of Ames Research Center.*

*This invention is owned by NASA, and a patent application has been filed. Inquiries concerning rights for the commercial use of this invention should be addressed to the Ames Technology Partnerships Division at (650) 604-2954. Refer to ARC-15475-1.*

# Probing a Spray Using Frequency-Analyzed Light Scattering

**Intact length and breakup frequency are determined by a relatively simple technique.**

*Marshall Space Flight Center, Alabama*

Frequency-analyzed laser-light scattering (FALLS) is a relatively simple technique that can be used to measure principal characteristics of a sheet of sprayed liquid as it breaks up into ligaments and then the ligaments break up into droplets. In particular, through frequency analysis of laser light scattered from a spray, it is possible to determine whether the laser-illuminated portion of the spray is in the intact-sheet region, the ligament region, or the droplet region. By logical extension, it is possible to determine the intact length from the location of the laser beam at the transition between the intact-sheet and ligament regions and to determine a breakup frequency from the results of the frequency analysis. Hence, FALLS could likely be useful both as a means of performing research on sprays in general and as a means of diagnostic sensing in diverse applications in which liquid fuels are sprayed. Sprays are also used for drying and to deposit paints and other coating materials.

Figure 1 depicts a laboratory setup for analyzing a spray by use of FALLS. A laser (or, in principle, any other suitable light source) generates a beam of light that is formed into a horizontal sliver by use of a beam-expanding lens and a cylindrical lens (the lenses are not shown in the figure). The spray to be analyzed is directed downward, and the sliver of light illuminates a thin probe volume that amounts, in effect, to a small cross section of the vertical spray. The principal characteristics of this region will be assessed. A rapid-response photodiode is positioned to receive forward-scattered light at an angle of 30° off the laser-beam axis. The output of the photodiode is digitized and frequency-analyzed by means of a fast Fourier transform (FFT). The nozzle and, thus, the spray can be translated vertically to enable optical probing of the spray at various axial distances from the nozzle.
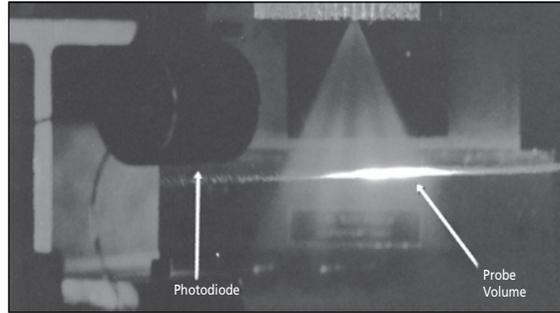


Figure 1. A **Horizontal Cross Section** of a vertically oriented conical spray is illuminated with a sheet of laser light. Light scattered off-axis from the laser beam is detected and frequency-analyzed.
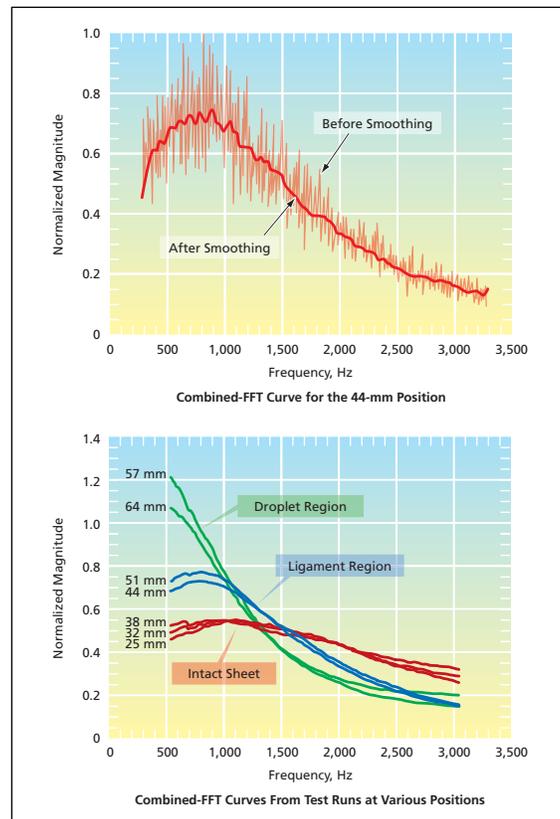


**Combined-FFT Curve for the 44-mm Position**

**Combined-FFT Curves From Test Runs at Various Positions**

Figure 2. **Normalized FFT Magnitude**s from the three spray regions of interest are clustered into distinct shapes representing the distinct frequency responses and their causative physical mechanisms in those regions.

In a series of tests in the setup of Figure 1, the technique was applied to a conical spray of water at a mass flow rate of 0.1 kg/s generated by use of a swirl coaxial injector nozzle with an upstream pressure of 830 kPa. Illumination power of 400 mW was generated by an argon-ion laser. The photodiode output was sampled at a rate of 20 kHz. Raw data were collected in sets of 4,096 samples (representing an observation interval of 0.2048 second per set). The spray was photographed with a stroboscope to obtain images of the spray for correlation with the FFT data. In addition, by use of phase Doppler anemometry, the spray speed 51 mm from the nozzle tip was estimated to be 14.2 m/s.

Each test run, lasting about 10 seconds, yielded 50 such sets. The 50 FFTs from each run were combined to obtain a single normalized FFT curve shown by the fluctuating thin curve shown in the upper part of Figure 2. A smoothing routine was invoked to suppress noise in the data, yielding the thick smoother curve shown superimposed on the thinner fluctuating one. Normalization was effected by dividing each FFT magnitude by the greatest magnitude in the noisy combined-FFT curve obtained from the test run in which the nozzle was positioned 44 mm above the light sheet. As shown in the lower part of Figure 2, the shapes of the normalized FFT curves were found to lie in three clusters corresponding to the intact-sheet, ligament, and droplet regions, respectively.

National Aeronautics and
Space Administration